World Applied Sciences Journal 11 (10): 1273-1281, 2010
ISSN 1818-4952

Calculation and Investigation of Temperature Distribution and Melt Pool Size Due to a Moving Laser Heat Source Using the Solution of Hyperbolic Heat Transfer Equation

[1]S. Saedodin, [1]M. Akbari, [2]A. Raisi and [1]M. Torabi

[1]Department of Mechanical Engineering, Semnan University, Semnan, Iran
[2]Department of Mechanical Engineering, Shahrekord University, Shahrekord, Iran

Abstract: In this paper, the melting of a semi-infinite body as a result of a moving laser beam has been studied. Because the Fourier heat transfer equation at short times and large dimensions does not have sufficient accuracy; a non-Fourier form of heat transfer equation has been used. Due to the fact that the beam is moving in x direction, the temperature distribution and the melting pool shape are not asymmetric. As a result, the problem is a transient three-dimensional problem. Therefore, thermophysical properties such as heat conductivity coefficient, density and heat capacity are functions of temperature and material states. The enthalpy technique, used for the solution of phase change problems, has been used in an explicit finite volume form for the hyperbolic heat transfer equation. This technique has been used to calculate the transient temperature distribution in the semi-infinite body and the growth rate of the melt pool. Temporal variation of laser beam intensity in two cases of continuous and pulsatile heat flux has been considered. The latter case is a model of electrical discharge machining (EDM). In order to validate the numerical results, comparisons were made with experimental data. Finally, the results of this paper were compared with similar problem that has used the Fourier theory. The comparison shows the influence of infinite speed of heat propagation in Fourier theory on the temperature distribution and the melt pool size.

Key words: Non-Fourier · Enthalpy technique · Melt pool · Radiational boundary condition

INTRODUCTION

Investigation of melting and solidification phenomena is important in most heat transfer engineering problems. For instance, in semiconductors producing technology, welding, found, crystallization and etc. The use of concentrated heat source energy such as laser and electrical discharge machining (EDM) are common nowadays in melting various materials. In all of problems like this, the solid and liquid phases are separated with an interface; interface developing in the solid or liquid phase, depends on both sides of the temperature gradients.

Rostami *et al.* [1] investigated the heating and melting of a semi-infinite body due to a stationary laser beam. Because the laser beam was stationary, the problem was assumed to be axisymmetric. The numerical solution was compared with experimental data and, because no vaporization occurred at the surface of the workpiece, reasonable agreement was seen.

Rostami and Raisi [2] studied the heating and melting of a semi-infinite body due to volumetric absorption of moving laser radiation. That was a transient three-dimensional conduction problem with a moving heat source and a moving phase boundary which was used with an explicit finite difference method. Temperature distribution and melt pool size for moving and a stationary laser beam were derived. In order to validate, the numerical solution was compared with experimental data. The comparisons showed that the numerical results were fairly accurate.

Sadd and Didlake [3] investigated the melting of a semi infinite solid in one dimensional based on non-Fourier heat conduction law postulated by Cattaneo [4] and Vernotte [5]. They confirmed that, unlike the classical Fourier theory which predicts an infinite speed of heat propagation, the non-Fourier theory implied that the speed of a thermal distribution is finite and the effect of this finite thermal wave speed on the melting phenomenon was determined. Finally they found out that, non-Fourier results differ from the Fourier theory only for small values of time.

Fangming jiang [6] investigated experiments on porous material heated by a microsecond laser pulse and the corresponding theoretical analysis. Some non-

Corresponding Author: S. Saedodin, Department of Mechanical Engineering, Semnan University, Semnan, Iran.
E-mail: s_sadodin@iust.ac.ir.

Fourier heat conduction phenomena were observed in the experimental sample. The experimental results indicated that only if the thermal disturbance be strong enough (i.e., the pulse duration is short enough and the pulse heat flux is great enough) it is possible to observe apparent non-Fourier heat conduction phenomenon in the sample and evident non-Fourier heat conduction phenomenon can only exist in a very limited region around the thermal disturbance position.

Abdel-jabbar *et al.* [7] investigated the thermal behavior of a thin slab under the effect of a fluctuating surface thermal disturbance, as described by the dual-phase-lag heat conduction model. It is found that, using the dual-phase-lag heat conduction model is essential at large frequencies of the surface disturbance. Mathematical criteria that specify the limits, beyond which both the hyperbolic wave and the dual-phase-lag heat conduction models deviate from the diffusion model, were obtained.

Formulation of the Problem: A review of literatures indicated that, all previous studied of the change-of-state heat transfer problems were based on the Fourier heat conduction law.

$$Q = -k\nabla T \tag{1}$$

Eq. (1) along with the conservation of energy gives the classical parabolic heat equation:

$$a\nabla^2 T = \frac{\partial T}{\partial t} \tag{2}$$

Many of the investigations indicated that Fourier's model possesses several serious shortcomings. The most prominent is that, this model implicates an infinite speed of heat propagation. Cattaneo and later Vernotte postulated a wave model for heat conduction in solids in the form below:

$$\frac{\partial q}{\partial t} + \frac{q_x}{\tau} = -\frac{k}{\tau}\frac{\partial T}{\partial x} \tag{3}$$

The quantity τ is called the material thermal relaxation time and is a physical result of a finite thermal communication time between material points.
The conservation energy equation is given by:

$$q_x = q_{x+dx} + \frac{\partial}{\partial t}(\rho cT)dV \tag{4}$$

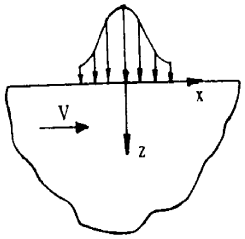

Fig. 1: Schematic representation of the problem in the two-dimensional case

Finally by using Cattaneo combination and conservation of energy equations, hyperbolic heat transfer equation may be expressed as:

$$\frac{\partial(\rho cT)}{\partial t} + \tau\frac{\partial^2(\rho cT)}{\partial t^2} + V\frac{\partial(\rho cT)}{\partial x} = \frac{\partial}{\partial x}(k\frac{\partial T}{\partial x}) + \frac{\partial}{\partial y}(k\frac{\partial T}{\partial y}) + \frac{\partial}{\partial z}(k\frac{\partial T}{\partial z}) + g \tag{5}$$

The corresponding volumetric heat generation is given by [8]:

$$g = -\frac{dI_a}{dz} = \alpha I_s(1-R)e^{-\alpha z} \tag{6}$$

Fig. 1 shows a schematic of semi-infinite body. Profile of the beam is considered circular and elliptical. The intensity of the beam that has Gauss' distribution may be expressed as [9]:

$$I_S(x,y,t) = I_0 h(t) e^{-\left[(x^2+y^2)/w^2\right]} \tag{7}$$

$$I_S(x,y,t) = I_0 h(t) e^{-\left[(x/w_x)^2+(y/w_y)^2\right]} \tag{8}$$

In last equations, w is the beam radius in the circular profile state; w_x and w_y are the beam radius in the x and y directions, in elliptical profile state. I_0 is the radiation intensity at the center of the beam and $h(t)$ stands for the temporal variation of the intensity. In the case of continuous heat flux, $h(t)$ has the constant value of unity, whereas in the pulsatile case it varies with time according to the following equation:

$$\begin{cases} h(t)=1 & if \quad 4(n-1)\Delta t \le t \le (4n-1)\Delta t \quad n=1,2,3,... \\ h(t)=0 & if \quad (4n-1)\Delta t \le t \le 4n\Delta t \end{cases} \tag{9}$$

The temporal variation of $h(t)$ in pulsatile case, according to the above relation, is shown in Figure 2:

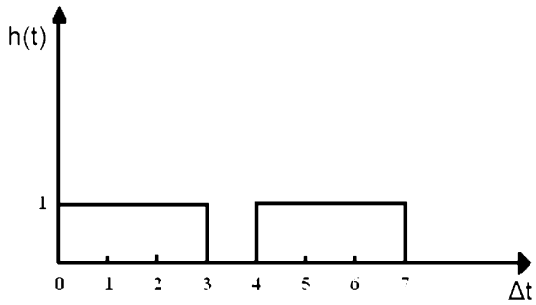

Fig. 2: Variation of $h(t)$ with respect to the time in pulsatile case

The local intensity of radiation decreases inside the material according to:

$$I_a = I_s(1-R)e^{-\alpha z} \tag{10}$$

Where R is the surface reflectivity and α is the absorption coefficient of the material.

Eq. (5) must be solved for the solid and liquid phase separately. The two solutions should then be related via the energy boundary conditions at the solid-liquid interface. The dependence of the position of the interface on the temperature distribution makes the problem complicated. One way to avoid this complexity is to write the left side of Eq. (5) in terms of enthalpy:

$$\frac{\partial e}{\partial t}+\tau\frac{\partial^2 e}{\partial t^2}+V\frac{\partial e}{\partial x}=\frac{\partial}{\partial x}(k\frac{\partial T}{\partial x})+\frac{\partial}{\partial y}(k\frac{\partial T}{\partial y})+\frac{\partial}{\partial z}(k\frac{\partial T}{\partial z})+g \tag{11}$$

In Eq. (11) e is term of enthalpy and may be expressed as:

$$e=\int \rho c dT \tag{12}$$

Initial and boundary condition

Initially, the temperature is equal to T_i everywhere:

$$at\ t=0: \quad T=T_i \tag{13}$$

Initially, the temperature variation is equal to zero

$$at \quad t=0: \quad \frac{\partial T}{\partial t}=0 \tag{14}$$

The boundary condition at the surface may be expressed as:

$$at \quad z=0: \quad -K\frac{\partial T}{\partial z}=\varepsilon(T)\sigma(T^4-T_\infty^4)+h(T-T_\infty) \tag{15}$$

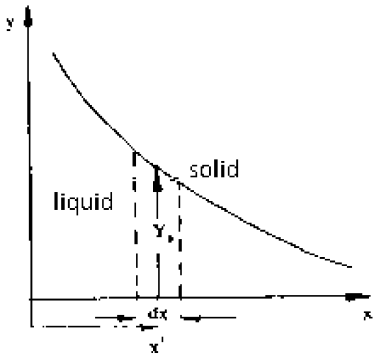

Fig. 3: Solid-Liquid interface in a two-dimensional view

Regions far from the source are supposed to be uninfluenced by the source

$$at \quad x\to\pm\infty: \quad T=T_i$$

$$at \quad y\to\pm\infty: \quad T=T_i \tag{16}$$

Conditions at the Interface: The energy balance at the interface is shown in Figure 3 may be written as [9]:

$$\left[1+(\frac{\partial X_s}{\partial y})^2+(\frac{\partial X_s}{\partial z})^2\right]\left[k_s\frac{\partial T_s}{\partial x}-k_\ell\frac{\partial T_\ell}{\partial x}\right]=L(\tau\frac{\partial^2 X_s}{\partial t^2}+\frac{\partial X_s}{\partial t}-V)$$

$$\left[1+(\frac{\partial Y_s}{\partial x})^2+(\frac{\partial Y_s}{\partial z})^2\right]\left[k_s\frac{\partial T_s}{\partial y}-k_l\frac{\partial T_\ell}{\partial y}\right]=L(\tau\frac{\partial^2 Y_s}{\partial t^2}+\frac{\partial Y_s}{\partial t}) \tag{17}$$

$$\left[1+(\frac{\partial Z_s}{\partial x})^2+(\frac{\partial Z_s}{\partial y})^2\right]\left[k_s\frac{\partial T_s}{\partial z}-k_\ell\frac{\partial T_l}{\partial z}\right]=L(\tau\frac{\partial^2 Z_s}{\partial t^2}+\frac{\partial Z_s}{\partial t})$$

Where X_s, Y_s Z_s indicate the coordinates of the interface in the x, y and z directions, also $\frac{\partial X_s}{\partial t}$, $\frac{\partial Y_s}{\partial t}$, $\frac{\partial Z_s}{\partial t}$ are the velocity components of the interface in the x, y and z directions, respectively. Once the enthalpy of each element is calculated, the following relations can be used to obtain the corresponding temperature [1]:

$$e_s=\int_{Tms}^{T}\rho_s c_s dT \qquad T_{ms}\le T$$

$$e_l=\int_{T_{ml}}^{T}\rho_l c_l\, dT+L \qquad T_{ml}\ge T \tag{18}$$

e_s, e_l are the amounts of the enthalpy in solid and liquid phases, respectively.

When an element contains both phases, x (i.e., the volume fraction of the liquid phase) must be calculated initially. The average enthalpy can be calculated afterward.

$$e = xe_l + (1-x)e_s \tag{19}$$

A procedure for the evaluation of the liquid fraction x will be introduced later.

For (ρc) an average value was assumed and by substitution e_s, e_l from Eq. (18) in Eq. (19), Eq. (20) can be written as follow:

$$e = xL + (\rho c)_{av}(T - T_m) \tag{20}$$

Where, T_m is melt temperature.

Thermophysical Properties: The thermophysical properties of the material were allowed to vary with temperature and phase state of the material. These properties for unalloyed aluminum may be expressed as [10, 11]:

Thermal conductivity coefficient $K(\frac{W}{m^\circ k})$

$$K_s = 226.67 + 0.033T \quad 300\,K < T \le 400K$$

$$K_s = 226.6 - 0.055T \quad 400K < T \le 933K$$

$$K_s = 63 + 0.03T \quad 933K < T \le 1600K$$

$$K_s = 114 \quad 1600K \le T \le 2723K \tag{21}$$

Specific heat at constant pressure $C_p(^{kj}/_{kgk})$

$$cp_s = 0.762 + 4.67 \times 10^{-4} \quad 300K < T \le 933K$$
$$cp_l = 0.921 \quad T > 933K \tag{22}$$

Density $\rho(^{kg}/_{m^3})$

$$\rho_s = 2767 - 0.22T \quad 300K < T \le 933K \tag{23}$$

Emissivity coefficient ε

$$\varepsilon = 7.2 \times 10^{-5}T + 3.5 \times 10^{-3} \tag{24}$$

Also, latent heat of diffusion is equal to:

$$L = 3.95 \times 10^5 \quad {}^{J}/_{kg} \tag{25}$$

By using these equations, e_s, e_l may be expressed as two polynomial functions in order 3 and 2, respectively.

$$e_s = 2108.454T + 0.5622T^2 - 3.4246 \times 10^{-5}T^3 - 2428827.8$$

$$e_l = 2431.44T + 0.12663T^2 + 9.4 \times 10^8 \tag{26}$$

$(\rho c)_{av}$ Can be expressed as:

$$(\rho c)_{av} = x(\rho c)_l + (1-x)(\rho c)_s \tag{27}$$

Which $(\rho c)_s$ and $(\rho c)_l$ are related to solid and liquid states, respectively.

By substituting Eq. (27) in Eq. (20), Eq. (20) can be written as follow:

$$e = xL + (3068.22 - 873.09x)(T - T_m) \tag{28}$$

In the numerical solution when an element contains only solid phase, the temperature can be calculated by applying the first term of Eq. (26), using the Newton-Raphson method. On the other hand, when an element contains only liquid phase, the temperature can be calculated by solution of polynomial function of order 2 in second term of Eq. (26). If an element contains two phases, Eq. (28) can be utilized to calculate the temperature.

Numerical Solution: In order to save computation time, the solution domain was divided into two regions: The inner region, which contains the liquid and/or solid state and the outer region, containing only the solid state. A fine mesh was used for the inner region, where the temperature gradients are large and the solid-liquid interface is present. The dimensions of the inner domain are smaller than outer region. On the basis of the work of Hsu and Mehrabian *et al.* [12] I_0w is an important parameter. If $I_0w < 1\times10^6$, the maximum temperature in the workpiece will not reach the boiling point of aluminum. Under this condition the maximum diameter of the melt pool is approximately $2.4w$ and depth of melt pool is nearly w for a stationary beam.

In numerical solutions often beam radius is considered about $100\mu m$. Based on these arguments, the diameter of the inner region will be 240 microns (μm). But because of moving heat source it was chosen to be 300 microns. The outer boundary of the computation domain was chosen such that conditions at infinity could be applied. The outer region radius usually is

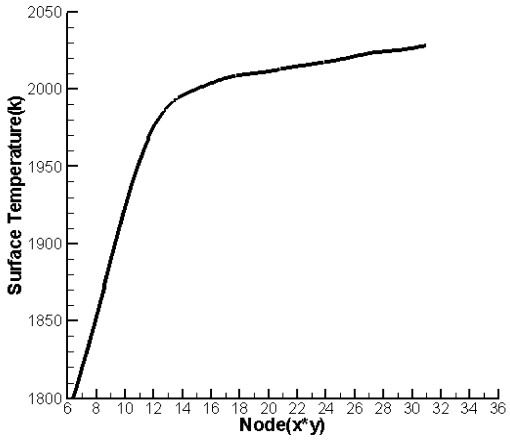

Fig. 4: Temperature variation of the surface central point versus number of the nodes

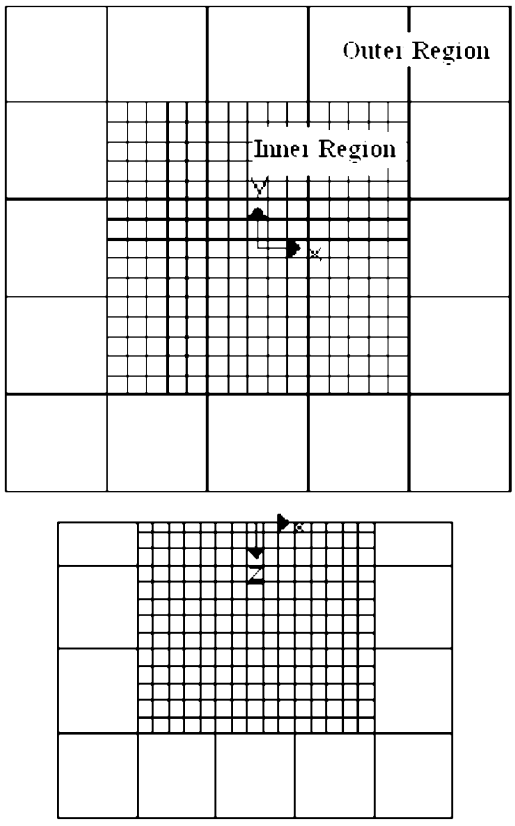

Fig. 5: Grid generation in x-y and x-z planes

considered as 20 times of the beam radius. Then for a beam with a radius of $100\mu m$ the R_0 can be calculated as follow:

$$R_0 = 20\times w = 2000\mu m \quad (29)$$

For determining the number of grids in the inner region, the grid study was used. First, the temperature of central point of body geometry versus the grid numbers was drawn in Figure 4. The results showed that temperature changing in 15th grid and higher can be assumed uniform and can be neglected. As a result, the grid numbers in inner region were considered as 15×15.

Grid numbers in z direction is considered as 13. Hence:

$$\Delta x_i = \Delta y_i = \frac{300}{15} = 20\mu m \quad , \quad \Delta z_i = 12\mu m \quad (30)$$

Each 5 internal grids are equivalent to one external grid. Therefore:

$$\Delta x_o = \Delta y_o = 5\times\Delta x_i = 100\mu m, \ \Delta z_\circ = 5\times\Delta z_i = 60\mu m \quad (31)$$

Finally, (15 ×15 ×13 = 2925) rectangular grids were used for the inner region and 57127 grids for outer region (Figure 5).

RESULTS AND DISCUSSION

In numerical solution of Eq. (11) in explicit finite volume form, the beam intensity was $I_0 = 3.5\times10^9 (W/m^2)$, the target velocity $Vw/2\alpha$, relaxation time $\tau = 0.2\times10^{-14}$ [13] and the beam radius was $100\mu m$. A pulse duration of $t_p = 1ms$ was used and initial temperature was $300K$.

Fig. 6 shows the maximum depth of the melt pool as a function of the beam intensity. It is assumed that the surface absorbs all of the beam energy. As it can be seen from Fig. 6, the numerical analysis is in good agreement with the experimental data, for low beam intensity. However, in the wake of the reaching to the vaporization threshold, the numerical analysis and experimental data are becoming further from each other.

Fig. 7 shows the depth of the melt pool as a function of the radius distance from the center of the beam. In this Fig. it can be seen that, there is negligible difference between numerical analysis and experimental data.

The temperature distribution of the center point as a function of time at various velocities is shown in Fig. 8. As it is observed, as much as the velocity of the beam increases, the temperature of the point decreases. This phenomenon is observed, due to the fact that as much as the velocity increases, the amount of energy that the specific point observes decreases.

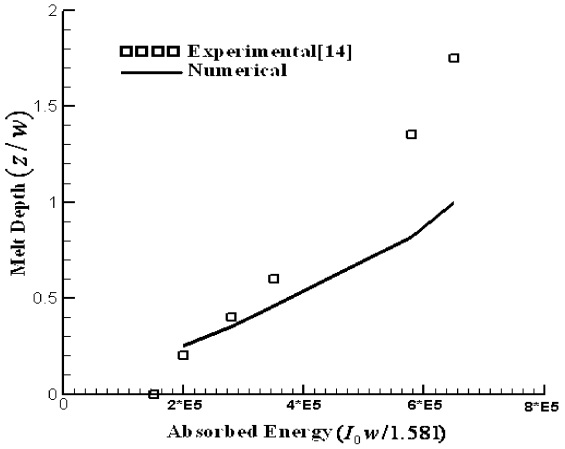

Fig. 6: Melting pool depth versus laser beam intensity at the center

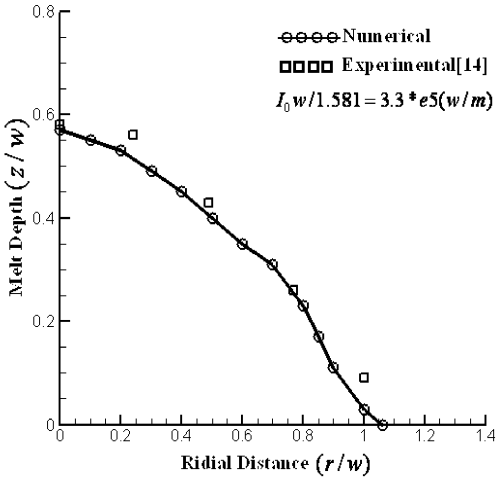

Fig. 7: Melting pool depth versus radial distance from the laser beam center

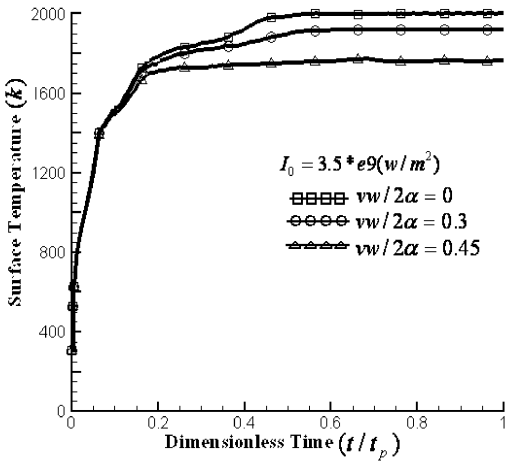

Fig. 8: Surface center point temperature with respect to the time at various speeds and intensity of $I_0 = 3.5\times 10^9$ (W/m^2) in continuous heat flux case

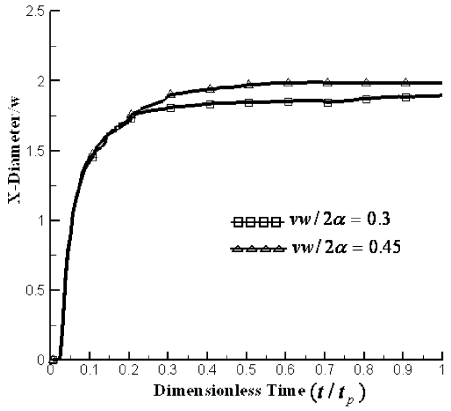

Fig. 9: Melting pool diameter on the x-axis with respect to the time for two different speeds in continuous heat flux case

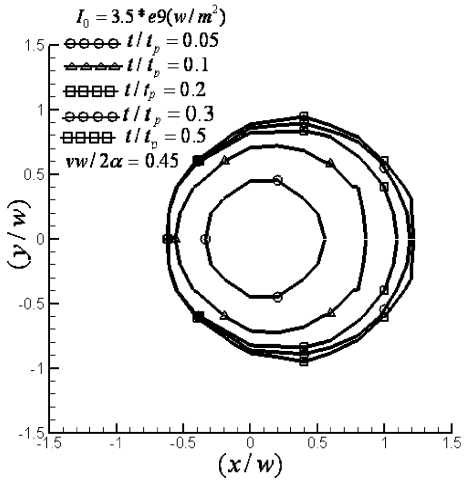

Fig. 10: Melting pool image on the x-y plane at a constant velocity and different times for a circular laser beam in continuous heat flux case

Fig. 9 shows the diameter of the melt pool along x direction at z=0. It can be seen that, as much as the velocity of the beam increases, the diameter of the melt pool along x direction increases slightly. On the other hand, by increasing the velocity of the beam, the diameter of the melt pool along y direction decreases.

The solid-liquid boundary of the melt pool in the xy plane for $Vw/2\alpha = 0.45$ is shown in Fig. 10. It can be perceived from Fig. 10 that, because of the moving beam, the melt pool tends to the right. Also, as time passes, the diameter of the melt pool increases and eventually it reaches to a specific value.

Fig. 11 shows the solid-liquid boundary of the melt pool in xz plane for $Vw/2\alpha = 0.3$. Due to the moving beam, the melt pool tends to the right.

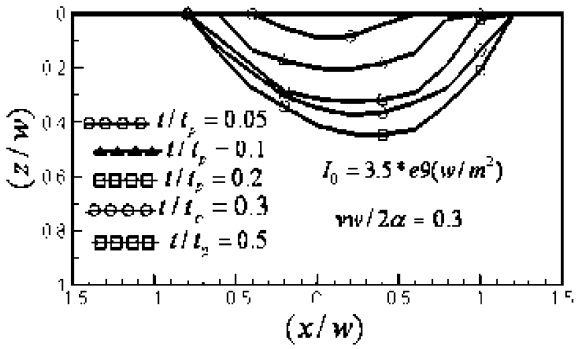

Fig. 11: Melting pool image on the x-z plane at a constant velocity and different times for a circular laser beam in continuous heat flux case

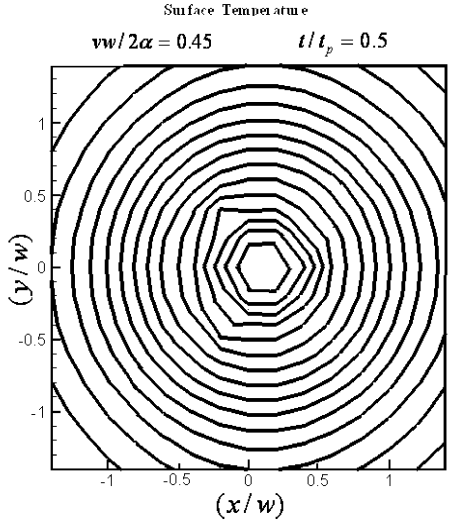

Fig. 12: Temperature contours in the x-y plane for circular laser beam in continuous heat flux case

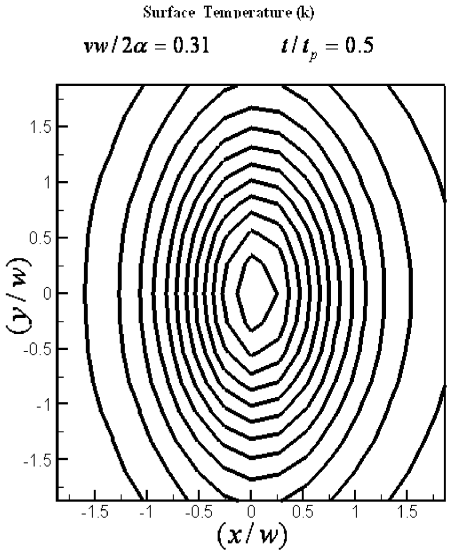

Fig. 13: Temperature contours in the x-y plane for elliptical laser beam in continuous heat flux case

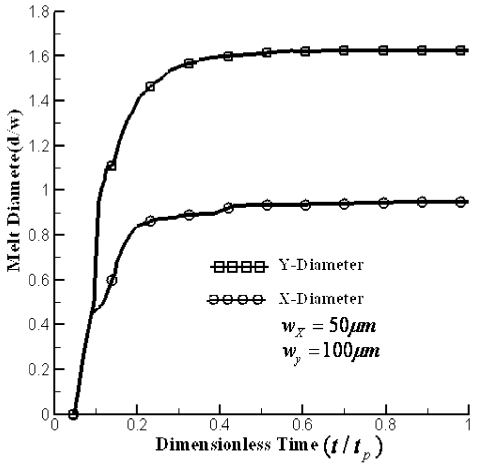

Fig. 14: Melting pool diameter on the x and y axes versus time for elliptical laser beam in continuous heat flux case

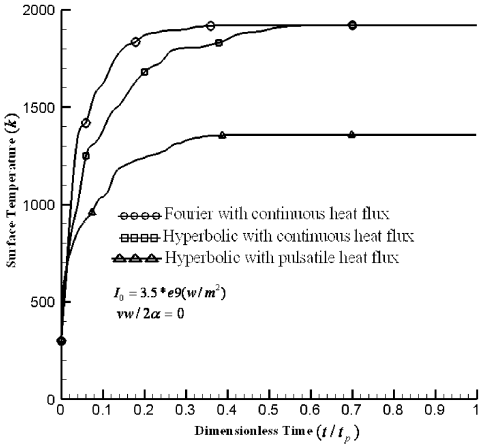

Fig. 15: Surface central point temperature versus time using Fourier and Hyperbolic methods

Fig. 12 shows the isotherm in xy plane for specific time and beam intensity, but for various beam velocity. The temperature fields are not symmetric due to the moving laser beam. It can be observed that, the temperature curves are more intensive at the left of the x direction.

Fig. 13 shows the isotherm in the xy plane when the elliptic beam is used.

The diameter of the melt pool along x and y directions are shown in Fig. 14, by using the elliptic beam.

Now, we are comparing the result of this paper and another paper, which has used fourier model.

Fig. 15 shows the temperature of the center point. It can be perceived from Fig. 14 that, the temperature of the center point increases faster, when the Fourier

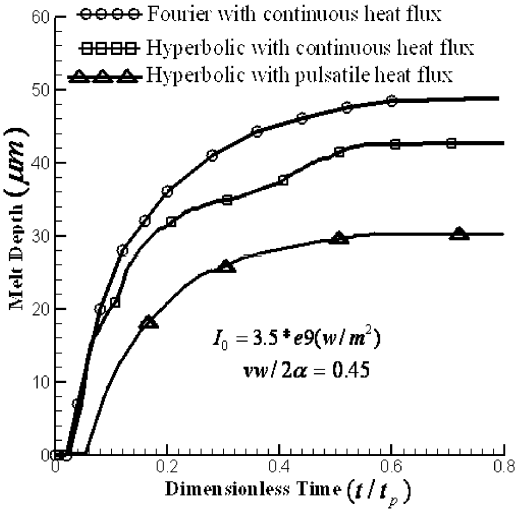

Fig. 16: Melting pool depth variation with time using Fourier and Hyperbolic methods

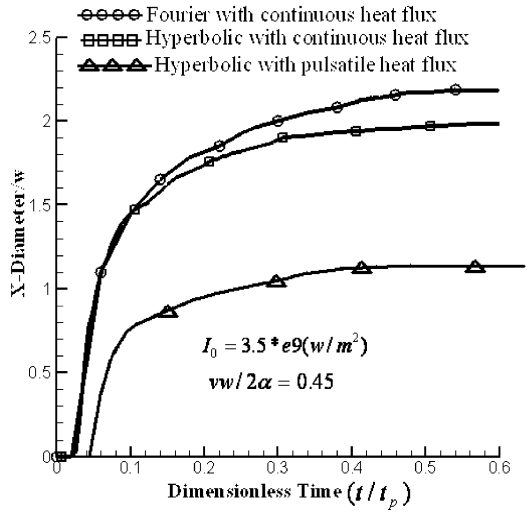

Fig. 17: Melting pool diameter on the x-axis versus time using Fourier and Hyperbolic methods

model is employed. But, the Fourier model and hyperbolic model reach each other by passing the time. This result was predictable, because the fourier and the hyperbolic models differ just in short times. The temporal variation of surface central point temperature for the pulsatile case is also shown in Fig. 15. The ultimate temperature of the central point in this case is less than that of the continuous case, which is due to lower value of total received energy from the laser beam radiation.

Fig. 16 shows the depth of the melt pool as a function of time for a dimensionless velocity (translational speed) of $Vw/2\alpha = 0.45$. As it can be observed from Fig. 16, in comparison to the other cases, the melt pool is deeper when Fourier heat conduction is applied.

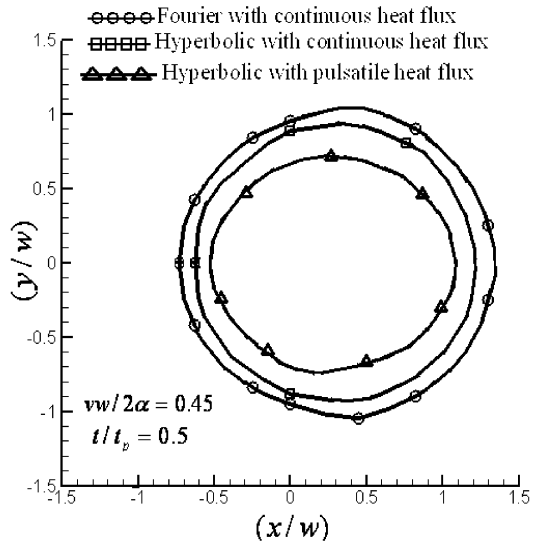

Fig. 18: Melting pool image on the x-y plane for a circular laser beam using Fourier and Hyperbolic methods

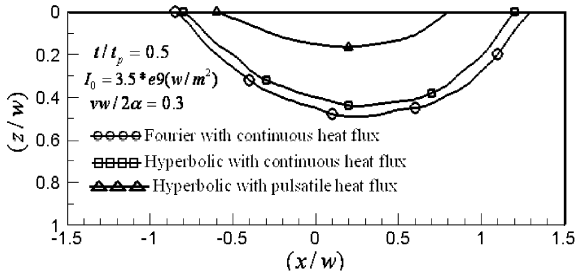

Fig. 19: Melting pool image on the x-z plane for a circular laser beam using Fourier and Hyperbolic methods

Also, the diameter of the melt pool along x direction at z=0 for dimensionless velocity $Vw/2\alpha = 0.45$, is shown in Fig. 17. It can be seen from this Fig. that, the diameter of the melt pool along x direction, using Fourier model, can increases faster and finally it reaches to a specific value.

The solid-liquid boundary in xy plane at $\frac{t}{t_p} = 0.5$ for $Vw/2\alpha = 0.45$ is shown in Fig. 18. As it can be predicted from Fig. 17, the size of the melt pool in xy plane when Fourier model is used, is greater than when the hyperbolic model with continuous and pulsatile heat flux is used.

Fig. 19 shows the solid-liquid boundary of the melt pool in xz plane at $\frac{t}{t_p} = 0.5$ for $Vw/2\alpha = 0.45$. According to Fig. 19 it can be concluded that, using Fourier model, the size of the melt pool in xz plane is greater than the same melt pool obtained from the hyperbolic model in the two continuous and pulsatile cases.

CONCLUSION

The temperature distribution and the size of the melt pool for an aluminum solid under the laser beam were studied. The hyperbolic heat equation was applied. The results of the hyperbolic model and the Fourier model were compared and it was seen that the increment of the melt pool and temperature fields were slower, when the hyperbolic model in continuous and pulsatile cases was applied. This phenomenon is in the wake of the infinite speed of the thermal waves in Fourier model. Also it was deduced that, the hyperbolic heat conduction model is suitable for short times and large domains and it can reached to the accurate results. In general, in practical applications such as electrical discharge machining (EDM), the pulsatile model has a better effectiveness than Fourier and continuous hyperbolic models.

AKNOWLEDGMENT

The authors gratefully acknowledge the support of the department of mechanical engineering and the office of gifted of Semnan University for funding the current research grant.

REFERENCES

1. Rostami, A.A., R. Greif and E.R. Russo, 1992. "Modified Enthalpy Method Applied to Rapid melting and solidification", Int. J. Heat Mass Transfer, 35(9): 2161-2172.
2. Rostami, A.A. and A. Raisi, 1997. Temperature distribution and melt pool size in a semi-infinite body due to a moving laser heat source, Numerical Heat transfer, Part A., 31: 783-796.
3. Sadd, M.H. and J.E. Didlake, 2001. Non- Fourier Melting of a same infinite solid, J. Heat Transfer, 2(81): 25-28.
4. Cattaneo, C., 1986. Form of conduction Equation Which Eliminates the Paradox of Instantaneous Propagation Compt. Rend., 247: 431-442.
5. Vernotte, P., 1986. Paradox in the Continuous Theory of Heat Equation Compt. Rend., 246: 3154-3159.
6. Fangming Jiang, 2002. Non- Fourier heat conduction phenomena in porous material heated by microsecond laser pulse, Taylor & Francis, 6: 331-346.
7. Abdel- Jabbar, N.M. and M.A. Ali Nimr, 2003. The Dual phase- lag heat conduction model in thin slab under fluctuating thermal disturbance, Taylor & Francis, 24: 47-54.
8. Rostami, A.A., R. Greif and E.R. Russo, 1990. "Unsteady two dimensional heat transfer in laser heated materials", processing, in Transport phenomena in Material, ASME Publication HID, pp: 146:
9. Raisi, A., 1995.Calculation of the temperature field and the melt pool shape due to laser heating (in Farsi), M.S. thesis, Isfahan University of technology, Isfahan, Iran.
10. Touloukian, Y.S. and C.Y. Ho, 1972. Eds, Thermophysical properties of Matters, Plenum Press, New York, 1(4).
11. Rohsenow, W.M. and J.P. Hartnett, (Eds), Handbook of heat transfer fundamentals, chap3, Mc Graw Hill, New York.
12. Mehrabian, R., S. Hsu, S.C. Kou and A. Munitz, 1982. Laser surface melting and solidification moving heat flux, metallurgical Trans, 14B: 213-227.
13. Neilw, 1975. Ashcroft and N. David. Mermin, Solid State Physics, pp: 10.